Available online at www.sciencedirect.com
ScienceDirect
Journal of Nuclear Materials 372 (2008) 312–317
journal of nuclear materials
www.elsevier.com/locate/jnucmat

Simulation of displacement cascades in $Fe_{90}Cr_{10}$ using a two band model potential

C. Björkas [a,*], K. Nordlund [a], L. Malerba [b], D. Terentyev [b], P. Olsson [c]

[a] Accelerator Laboratory, University of Helsinki, P.O. Box 43, FI-00014, Finland
[b] SCK·CEN, The Belgian Nuclear Research Centre, Boeretang 200, B-2400 Mol, Belgium
[c] Departément Matériaux et Méchanique des Composants, Electricité de France, Les Renardières, F-77250 Moret-sur-Loing, France

Received 19 September 2006; accepted 22 March 2007

Abstract

Molecular dynamics (MD) simulations of displacement cascades, with recoil energies up to 50 keV, have been performed in $Fe_{90}Cr_{10}$ and Fe using a recently developed two band embedded atomic model (2BM) potential that correctly describes the mixing enthalpy and the binding energy of the mixed dumbbell configurations. Comparisons between results obtained with the 2BM potential fitted to different data sets, a one band model (1BM), and another existing FeCr-potential previously used for similar calculations were done, showing differences in the vacancy clustered fraction and the Cr content in interstitials predicted by the potentials. The 2BM potential resulted in roughly the same concentration of Cr in interstitial positions as in the matrix, and the 1BM, which incorrectly predicts a positive heat of mixing, predicted even smaller concentrations. The calculated short range order parameter is around zero for the 2BM, and takes positive values within the 1BM, as expected from the mixing enthalpies.

PACS: 61.72.Ji; 61.80.Hg; 28.52.Fa; 34.20.Cf

1. Introduction

Due to their high swelling resistance and thermal conductivity, ferritic/martensitic steels are considered as possible components in nuclear applications such as fusion reactors [1,2]. However, their behavior under the irradiation conditions expected in such nuclear systems, is difficult to test due to the absence of facilities capable of reproducing the combined influence of fast neutron flux, large fluence, high temperature and stresses. Therefore the behavior is not yet fully understood. Equally hard to explain is the effect that Cr-concentration, the irradiation dose and temperature have on the mechanical properties and swelling of these steels [1,3,4]. Studies at the atomic level, including molecular dynamics (MD) simulations of displacement cascades, are thus required to achieve the necessary understanding of the mechanisms behind the macroscopic behavior of these materials during and after irradiation.

Since experiments have shown that the Cr concentration plays a crucial role on the radiation hardness of steels, FeCr-alloys are the simplest alloys to be used as model materials when studying the basic mechanisms governing their behavior under irradiation. The reliability of atomistic simulations is highly dependent on the potential describing the interactions between the atoms, whence there is a constant push for more accurate potentials to be developed. Despite the huge interest in FeCr-alloys, just a few studies of displacement cascades have been done in this system, for instance Refs. [5–7]. Different potentials applicable to FeCr have been developed [8–11]. Some of them [8,9] have, however, shortcomings, including an incorrect description of the stable interstitial configurations, of the interaction energy between a chromium and an self interstitial atom (SIA), and of the behavior of the mixing enthalpy

* Corresponding author.
E-mail address: carolina.bjorkas@acclab.helsinki.fi (C. Björkas).

0022-3115/$ - see front matter © 2007 Elsevier B.V. All rights reserved.
doi:10.1016/j.jnucmat.2007.03.265

curve according to *ab initio* data [12]. The enthalpy curve is experimentally [13] and by *ab initio* calculations [14] seen to exhibit a change of sign, going from negative to positive values at a certain critical Cr concentration between 8 and 10%. Olsson et al. have developed a two band model (2BM) potential [15] which correctly reproduces the Fe–Cr mixing for all Cr concentrations. This potential was also fitted to reproduce the Cr–SIA interaction as closely as possible. A recent potential, developed by Caro et al. [11], has got similar thermodynamic capabilities, but is not optimized for the Cr–SIA interaction.

In this study we are testing the 2BM potential, by comparing results of collision cascades in $Fe_{90}Cr_{10}$ with results obtained using the same model but without the second band, i.e. a one band model (1BM), the potential by Chakarova et al. (here referred to as CWP) [6,10] and cascades in pure Fe. We are also discussing the possible longer-term development of the system and the cascade induced short range order (SRO) parameter [16] of the alloy. A positive value of the SRO parameter indicates that Cr atoms prefer being close to each other whereas a negative value means the opposite, thereby resulting in ordering in the alloy. If the parameter equals zero, the Cr atoms are randomly distributed in the alloy. The SRO parameter correlates with the mixing enthalpy, thus also showing negative values below a critical Cr-concentration of about 10%. We investigate whether, starting from random alloys, the cascade is capable of producing a change in the local SRO.

The chromium content of 10% is of particular interest since it is close to that used in nuclear applications and the critical concentration is around this value. Moreover, the CWP, used for simulating cascades and for comparison, was fitted to properties of $Fe_{90}Cr_{10}$. For these reasons, the concentration of chromium was set to this value in the current work.

2. Method

The main focus of this work is given to the interatomic potential developed by Olsson et al. [15] as described above. The second band part of the potential can, however, be left out. The resulting 1BM, which alone can not guarantee good fitting to the FeCr properties, turns out to have a clearly positive heat of mixing, allowing for testing its effect on the results.

The pair interaction and the many-body functionals for Fe in the 2BM potential were developed by Ackland et al. [17] and the potential for Cr by Olsson et al. [15,18,19]. The density function in the Cr potential has the same shape as the one used for Fe. The coefficients of the alloy potential were fitted to the lattice parameter of $Fe_{90}Cr_{10}$, a positive heat of mixing for equimolar composition, the binding energy of the mixed $\langle 1\,1\,0\rangle$-dumbbell in bulk Fe, the substitution energy of a Cr atom in bulk Fe, and the mixing enthalpy curve.

Since two somewhat different sets of data for the substitution energies and mixing enthalpy exist, obtained by two different *ab initio* methods, namely the exact muffin-tin orbital (EMTO) method [20], and a method that used the projector augmented wave (PAW) formalism [21,22], two potentials, here denoted as the EMTO and PAW potentials, were actually fitted. The details of the two data sets are found in Ref. [23].

The cascade simulations were performed with the MD code PARCAS [24]. In the $Fe_{90}Cr_{10}$ simulations using the 2BM potential and in pure Fe, the recoil energies ranged from 0.5 keV up to 50 keV. The upper energy limit in the corresponding 1BM-simulations was 20 keV and only 5 keV-recoils were used within the CWP. However, the results obtained with the CWP have been combined with those already published in Ref. [6]. These were obtained with completely independent MD and analysis methods. The simulations at 5 keV were used to demonstrate the equivalence and compatibility between the published results [6] and those produced in this work. The size of the simulation cell, number of runs, and the number of atoms in the cells for each recoil energy and potential used in this work are found in Table 1.

Periodic boundary conditions [25] were used at the simulation cell borders in all three dimensions and no electronic stopping was used for consistency with the simulations done in [6]. The simulation cells were initially thermally equilibrated at 300 K for 10 ps. Berendsen pressure control [26] was used to keep the cell at zero pressure during this initial simulation.

The thermally equilibrated simulation cell was then used for the recoil calculations. The recoil energy and a random direction was given to an Fe atom near the center of the cell. In these simulations, Berendsen temperature control [26] with a time constant of 100 fs was used to scale the temperature at the cell boundary, the thickness of which was taken to be two lattice constants. The movement of the atoms was monitored in such a way that, if the energy of any atom in the border region exceeded 10 eV, the simulation was stopped, and then re-started with an initial recoil position placed further away from the border but keeping the recoil direction the same. This monitoring was, however, not done in the 50 keV-cascades since this would have required an enormous cell, which in turn would have resulted in time consuming simulations. A visual inspection showed that the 50 keV cascades were not overlapping even if passing over the periodic boundaries.

A Wigner–Seitz (WS) cell [27], centered on each lattice site, was used to identify vacancies and interstitial atoms. An empty cell corresponded to a vacancy and two or more atoms in the same cell were defined as an interstitial.

A cluster analysis was also performed. For vacancies, the cut-off radius for cluster connectivity was chosen to be the second nearest neighbor distance. The radius for interstitial clusters was the third nearest neighbor distance. These particular cut-offs equal those used in the analysis in Ref. [6] in order to make comparisons easier.

The chromium content among interstitials was analyzed in two different ways. The fraction of Cr atoms among all

Table 1
The recoil energies, time of simulation, number of events, box size, and number of atoms used in the recoil cascade simulations in this work

Energy (keV)	Simulation time (ps)	Number of events $Fe_{90}Cr_{10}$			Fe	Box size (a_0)	Number of atoms
		EMTO	PAW	1BM EMTO			
0.5	20	20	20	20	20	20	16000
1	20	20	20	20	20	25	31250
2	20	20	20	20	20	31	59582
5	20	100	100	15	100	42	148176
10	25	15	15	15	15	54	314928
20	25	15	15	15	25	67	601526
50	30	10	10	–	4	90	1458000

interstitial atoms as well as the fraction of interstitials that contain at least one Cr atom was calculated. The same was done for interstitial clusters: the fraction of Cr atoms among clustered interstitial atoms was obtained and also the fraction of clusters that contained Cr atoms.

3. Results and discussion

3.1. Comparison between models

In order to compare the method for scaling the temperature at the borders with that of no temperature control (an approach frequently employed in other works [6,28,29]), simulations using the 2BM potential fitted to EMTO-data without the scaling were also done. Fifteen cascades were simulated. The results showed that, within the statistical uncertainties, the two methods gives practically identical results. For instance, the number of Frenkel pairs, produced by 5 keV cascades, when no temperature control was applied was 15.9 ± 1.1, (with T-control: 15.4 ± 0.4), the fraction of clustered interstitials $39 \pm 6\%$ ($33 \pm 5\%$) and the fraction of chromium in interstitial atoms $12 \pm 2\%$ ($11.6 \pm 0.7\%$). The uncertainties correspond to the standard deviation of the average.

A comparison between the results of the analysis performed on final atom positions after 5 keV cascades simulations in $Fe_{90}Cr_{10}$ with the different potentials, including results for the CWP obtained with two different MD codes, can be seen in Table 2. Results for simulations in pure Fe are also shown.

All the results for the CWP provided by Terentyev et al. [6] using the DYMOKA code [29] and the simulations done in this work, are similar. The number of Frenkel pairs (FPs) produced in $Fe_{90}Cr_{10}$ is, within the statistical uncertainties, also equal for all the FeCr potentials, and slightly higher than in Fe. Note that performing simulations in pure Fe means here using only the Ackland–Mendelev (AMS) potential [17], since this is the Fe-part of the 2BM potential. Simulations of cascades with the AMS potential have been carried out in a previous work [30] and the results of that study are in close agreement with these.

In particular, the 2BM and 1BM potentials estimate a larger fraction of vacancies in clusters when compared to the CWP, a phenomenon that can be ascribed to the differences in the Fe–Fe interaction description between the CWP and AMS potentials. This has already been observed and discussed in Ref. [30]. A comparison of the Cr content in the interstitials also reveals some differences between the potentials, since the CWP gives a larger estimate of the fraction of Cr atoms in both clustered and total amount of interstitial atoms than the other potentials. The 2BM results in a fraction of Cr in interstitials which is almost the same as in the matrix, whereas the 1BM shows even lower concentrations. This behavior is due to the 1BM hav-

Table 2
Comparison between defects produced by 5 keV cascades in Fe and $Fe_{90}Cr_{10}$ with different potentials

			$Fe_{90}Cr_{10}$			Fe
Potential	CWP	CWP	2BM	2BM	1BM	AMS
Version			EMTO	PAW	EMTO	
Number of events	10	15	100	100	15	100
MD Code	DYMOKA			PARCAS		
Frenkel pairs	13 ± 3	14.9 ± 0.9	15.4 ± 0.4	15.3 ± 0.6	13.7 ± 1.0	14.4 ± 0.4
Vacancy clustered fraction (%)	27 ± 4	25 ± 5	42 ± 4	43 ± 2	39 ± 6	40 ± 3
Interstitial clustered fraction (%)	38 ± 10	40 ± 7	33 ± 5	34 ± 2	35 ± 2	32 ± 2
Frac. of Cr among interstitial atoms (%)	41 ± 10	41 ± 4	11.6 ± 0.7	12.8 ± 0.9	2.7 ± 0.9	
Frac. of interstitials with Cr (%)		73 ± 6	23 ± 2	27 ± 2	11 ± 3	
Frac. of Cr among clustered int. atoms (%)	20 ± 5	30 ± 8	9.2 ± 1.3	10.1 ± 1.3	2.5 ± 1.5	
Frac. of clustered int. which contain Cr (%)		55 ± 15	17 ± 3	20 ± 3	5 ± 3	

CWP refers to the potential by Chakarova et al. [10], 2BM is the two band model of Olsson et al. [15] and 1BM is the 2BM with the second band part removed. EMTO and PAW are versions of the 2BM fitted to two different data sets and AMS refers to the Fe-part of the 2BM [17].

Table 3
Characteristic interstitial energies in eV for Cr atoms(s) in an iron lattice with the 2BM potentials fitted to EMTO-data

	2BM EMTO	1BM EMTO
$E^{\text{Fe–Cr}}_{\langle 1\,1\,0\rangle} - E^{\text{Fe–Fe}}_{\langle 1\,1\,0\rangle} - E^{\text{Cr}}_{\text{sub}}$	+0.13	−0.11
$E^{\text{Fe–Cr}}_{\langle 1\,1\,1\rangle} - E^{\text{Fe–Fe}}_{\langle 1\,1\,1\rangle} - E^{\text{Cr}}_{\text{sub}}$	+0.38	+0.065
$E^{\text{Cr–Cr}}_{\langle 1\,1\,0\rangle} - E^{\text{Fe–Fe}}_{\langle 1\,1\,0\rangle} - 2E^{\text{Cr}}_{\text{sub}}$	−0.46	+0.24
$E^{\text{Cr–Cr}}_{\langle 1\,1\,1\rangle} - E^{\text{Fe–Fe}}_{\langle 1\,1\,1\rangle} - 2E^{\text{Cr}}_{\text{sub}}$	−0.24	−0.014

And corresponding 1BM (qualitatively similar results were found with the PAW-fitted 2BM). A positive value indicates a bound defect configuration.

ing a negative interaction energy for a mixed Fe–Cr $\langle 1\,1\,0\rangle$-dumbbell when compared to a pure Fe–Fe one (see Table 3).

3.2. Results for different energies

The results of the cascade simulations in the whole energy range can be seen in Figs. 1–7. The figures show data obtained using both versions of the 2BM model and the artificial 1BM potentials fitted to EMTO-data as well as, for direct comparison, results obtained with the CWP and the DYMOKA code [6] (Figs. 1 and 3–6). The Figs. 1–5 also include results from the Fe-simulations.

Fig. 1 shows the number of FPs as a function of recoil energy. A power-law behavior, aE^{b}_{rec}, with essentially coincident constants in all cases, can be observed. The evolution with time of the FPs in the 10 keV cascades can be seen in Fig. 2, which shows the peak time being around 750 fs. The number of defects becomes stable after roughly 10 ps and the absence of the second band does not have any effect on the total defect production.

The fraction of vacancies and interstitials in clusters is illustrated in Figs. 3 and 4, respectively. The vacancy cluster fraction ranges from about 40–55% for the 2BM and are within uncertainties the same for the 1BM. The results for Fe are in the same range. With the CWP, on the other hand, a smaller fraction is obtained, as a consequence of

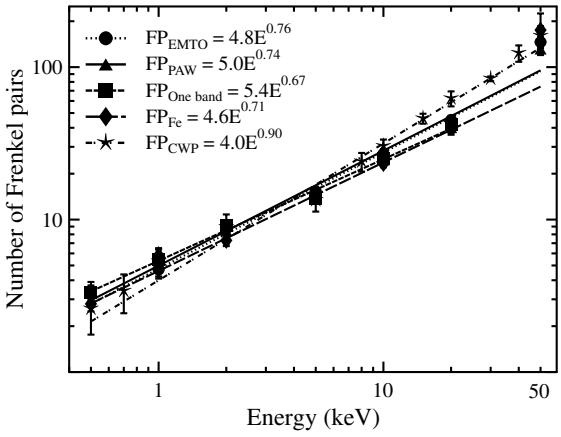

Fig. 1. Number of Frenkel pairs (FPs) at the end of recoil collision cascades in $Fe_{90}Cr_{10}$ with different potentials, and in pure Fe.

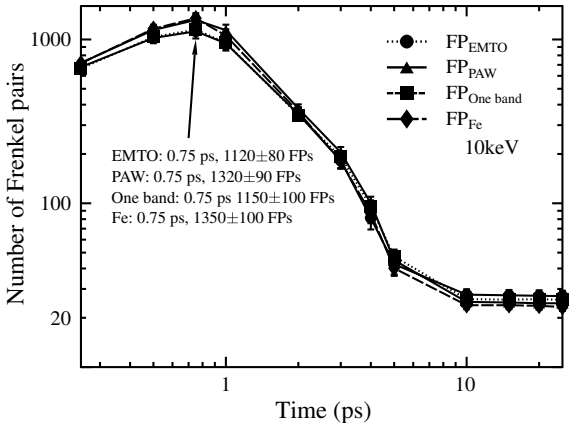

Fig. 2. Average number of Frenkel pairs (FPs) as a function of time during 10 keV-cascades in $Fe_{90}Cr_{10}$ and Fe.

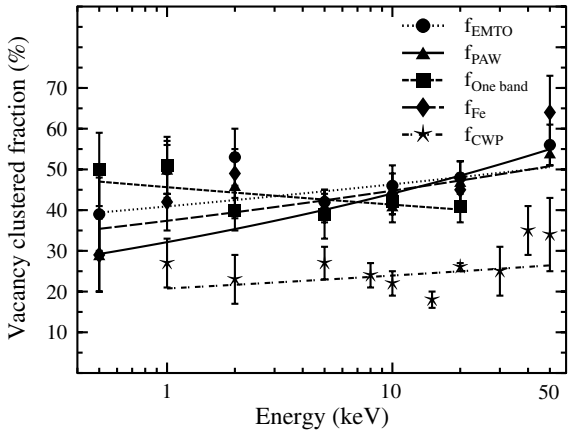

Fig. 3. Fraction (f) of vacancies in clusters as a function of recoil energy. Data is shown for different potentials in $Fe_{90}Cr_{10}$ and for simulations in Fe.

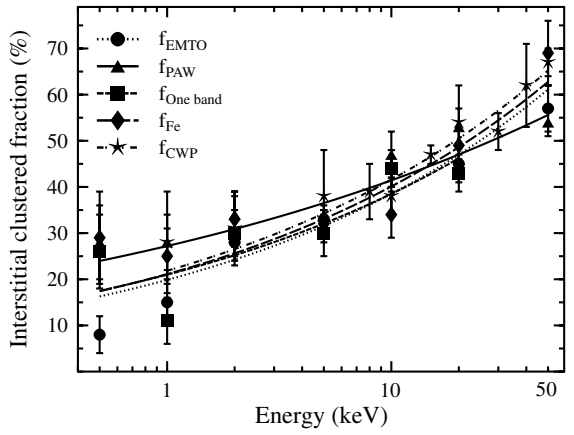

Fig. 4. Fraction (f) of interstitials in clusters as a function of recoil energy. Data from simulations using different potentials in $Fe_{90}Cr_{10}$ and from simulations in pure Fe is shown.

the different features of the corresponding Fe–Fe potentials [6,30]. The interstitial cluster fraction is growing linearly

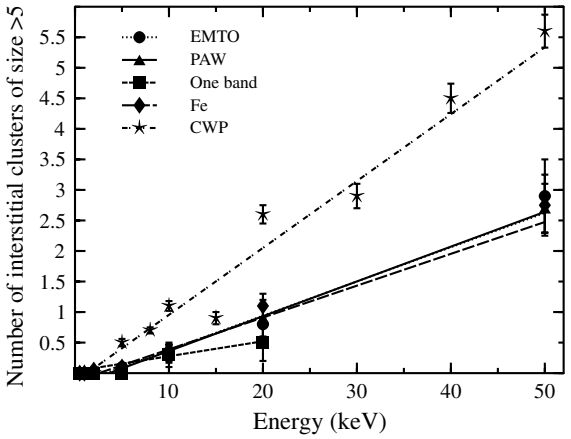

Fig. 5. The number of interstitial clusters with more than five defects as a function of recoil energy.

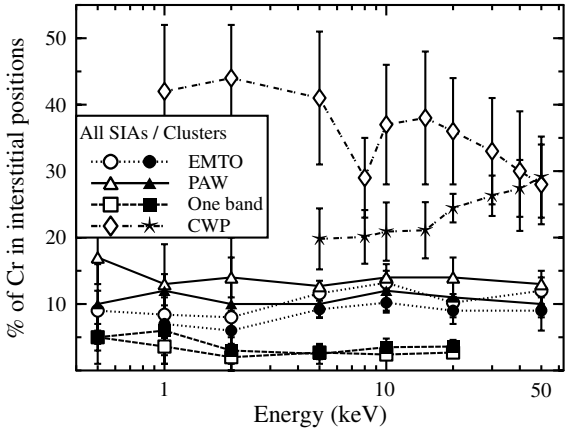

Fig. 6. Fraction of Cr in all (empty markers) and in clustered (filled markers) interstitial atoms (SIAs) as a function of recoil energy.

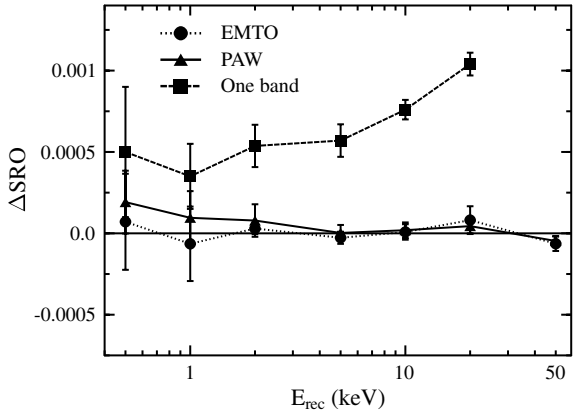

Fig. 7. Change in the short range order parameter in $Fe_{90}Cr_{10}$ during cascades with the EMTO and PAW versions of the two band model, and the one band model.

with recoil energy, being above 50% after 50 keV-cascades. Again, the 2BM and 1BM behave similarly to each other, to pure Fe, and in this case also to the CWP.

Fig. 5 shows the amount of interstitial clusters containing more than five defects. The CWP resulted in a larger amount of these kinds of clusters than the EMTO, PAW and the AMS potentials, which show an identical behavior.

The effect of the second band is easily deduced from Fig. 6. This figure illustrates the chromium content in interstitial atoms and in clustered interstitial atoms. The overall trend is that the chromium content is much smaller within the 1BM, as expected from the defect formation energies (see Table 3). In this case the CWP outcome is largely different and the association of SIAs to Cr is found to be spectacular in this potential. The reasons for these differences will be discussed in Section 3.3. Noticeable is also the fact that the Cr fractions within the PAW-version are clearly above the matrix concentrations at low energies.

The negative binding energy of the Fe–Cr ⟨1 1 0⟩-dumbbell configuration in the 1BM, explains the low concentration of Cr in interstitials predicted by this potential.

The SRO parameter was calculated inside the second nearest neighbor shell. Although being close to zero, the SRO-value of the relaxed simulation cell was subtracted from the final value after the cascades in order to be sensitive to even small variations. The calculations resulted in the values shown in Fig. 7. The SRO variations for the 2BM potential are approximately zero after the different displacement cascades. The 1BM, on the other hand, predicts positive values, indicating that local chromium clustering is taking place and proving that the time frame of the cascade development is in principle sufficient to trigger phase transformations. Phase transitions in alloys occurring during cascade time scales have earlier been reported in FCC metal alloys [31,32], but since cascades in BCC metals are less dense, it is not *a priori* clear that similar effects could occur in them. Thus, although the 2BM results show that changes in the SRO are not likely in true $Fe_{90}Cr_{10}$ (which has essentially zero heat of mixing), the 1BM result suggests that it might well occur in FeCr alloys with other Cr concentrations. For instance, it would be interesting to study $Fe_{95}Cr_5$ or $Fe_{80}Cr_{20}$, with clearly non-zero heats of mixing, to find out whether changes in the SRO can occur in them already on cascade time scales.

3.3. Implications on longer-term evolution

The simulations performed with the 2BM potentials show that chromium interstitials are not enriched directly in the cascades. In contrast, the results obtained with the CWP show a spectacular Cr enrichment of SIAs, especially isolated. The reason for this discrepancy is that the single SIA in the CWP has the ⟨1 1 1⟩-crowdion structure and can easily glide in 1D to the closest Cr atom within the cascade time limits. Thus, most SIAs will end up becoming mixed dumbbells. The same behavior is exhibited by clusters of all sizes within this potential. On the contrary, the AMS potential predicts higher migration energies and 3D migration paths. The binding energies found in Table 3 imply, indeed, that Fe–Fe interstitials in the vicinity of

Cr atoms will become Cr-enriched in the 2BM potentials when the system evolves further. The concentration of Cr in interstitials is thus expected to grow.

All in all, one can assume that the different potentials' description of Cr associated with clusters will become more similar on a longer timescale.

4. Conclusions

Analyses of displacement cascades in $Fe_{90}Cr_{10}$ and Fe, with recoil energies ranging between 0.5 and 50 keV, have been carried out paying special attention to the behavior of the produced defects when using a recent two band model (2BM) potential constructed for FeCr-alloys. Comparisons between results of simulations using two slightly different versions of the 2BM, an artificial one band model (1BM) of the same, another available FeCr potential (CWP) and with simulations in pure Fe were done.

The defect analysis revealed no significant differences between the two 2BM versions. According to these potentials, the chromium content in interstitial defects is essentially the same as in the initial matrix, something which differs from the predictions of CWP, where this content is considerable. The differences are attributed to the different description of single interstitial and interstitial cluster mobility predicted by the corresponding Fe potentials. The CWP also resulted in a lower vacancy clustered fraction than the 2BM.

The chromium concentration in defects is, however, likely to grow with time in the 2BM due to the attractive energies of the mixed dumbbell predicted by the potential.

Even lower chromium concentrations in defects were found when using the 1BM, which was obtained by removing the second band term. Simulations with this model also showed that the cascade time frame is sufficient to trigger phase transformations, Cr clusters in the present case.

Comparisons with pure Fe simulations showed that the 2BM applied to $Fe_{90}Cr_{10}$ gives similar results with respect to the total damage production and defect clustering as in Fe.

Acknowledgements

This work, supported by the European Communities under the contract of Association between EURATOM/Tekes, was carried out within the framework of the European Fusion Development Agreement. The views and opinions expressed herein do not necessarily reflect those of the European Commission. The research was performed within the Finnish Centre of Excellence in Computational Molecular Science (CMS), financed by The Academy of Finland and the University of Helsinki.

References

[1] R. Klueh, K. Ehrlich, F. Abe, J. Nucl. Mater. 191–194 (2002) 116.
[2] A. Kohyama, A. Hishinuma, D. Gelles, R. Klueh, K. Ehrlich, J. Nucl. Mater. 233–237 (1996) 138.
[3] F. Garner, M. Toloczko, H. Sencer, J. Nucl. Mater. 276 (2000) 123.
[4] B. Sencer, F. Garner, J. Nucl. Mater. 283–287 (2000) 164.
[5] D. Terentyev, L. Malerba, M. Hou, Nucl. Instrum. and Meth. B 228 (2005) 156.
[6] D. Terentyev, L. Malerba, R. Chakarova, C. Domain, K. Nordlund, P. Olsson, M. Rieth, J. Wallenius, J. Nucl. Mater. 349 (2006) 119.
[7] J.-H. Shim, H.-J. Lee, B.D. Wirth, J. Nucl. Mater. 351 (2006) 56.
[8] D. Farkas, C.G. Schon, M.S.F. de Lima, H. Goldstein, Acta Mater. 44 (1996) 409.
[9] T. Konishi, K. Ohsawa, H. Abe, E. Kuramoto, Comput. Mater. Sci. 14 (1999) 108.
[10] R. Chakarova, V. Pontikis, J. Wallenius, Development of fe(bcc)cr many body potential and cohesion model, Delivery Report WP6, SPIRE Project, EC Contract No. FIKW-CT-2000-00058, Available at <http://www.neutron.kth.se/publications>.
[11] A. Caro, D.A. Crowson, M. Caro, Phys. Rev. Lett. 95 (7) (2005) 075702.
[12] P. Olsson, L. Malerba, A. Almazouzi, SCK-CEN Report BLG-950.
[13] I. Mirebeau, M. Hennion, G. Parette, Phys. Rev. Lett 53 (7) (1984) 687.
[14] P. Olsson, I. Abrikosov, J. Wallenius, Phys. Rev. B 73 (2006) 104416.
[15] P. Olsson, J. Wallenius, C. Domain, K. Nordlund, L. Malerba, Phys. Rev. B 72 (2005) 214119.
[16] J. Cowley, Phys. Rev. 77 (5) (1950) 669.
[17] G.J. Ackland, M.I. Mendelev, D.J. Srolovitz, S. Han, A.V. Barashev, J. Phys.: Condens. Mat. 16 (27) (2004) S2629.
[18] J. Wallenius, P. Olsson, C. Lagerstedt, N. Sandberg, R. Chakarova, V. Pontikis, Phys. Rev. B 69 (2003) 094103.
[19] J. Wallenius, P. Olsson, C. Lagerstedt, Nucl. Instrum. and Meth. B 228 (2005) 122.
[20] O. Andersen, T. Saha-Dasgupta, Phys. Rev. B 62 (2000) R16219.
[21] G. Kresse, D. Joubert, Phys. Rev. B 59 (1999) 1758.
[22] P. Blöchl, Phys. Rev. B 50 (1994) 17953.
[23] P. Olsson, I. Abrikosov, L. Vitos, J. Wallenius, J. Nucl. Mater. 321 (2003) 84.
[24] PARCAS computer code. The main principles of the molecular dynamics algorithms are presented in [33,34]. The adaptive time step and electronic stopping algorithms are the same as in [35].
[25] M.P. Allen, D.J. Tildesley, Computer Simulation of Liquids, Oxford University Press, Oxford, England, 1989.
[26] H.J.C. Berendsen, J.P.M. Postma, W.F. van Gunsteren, A. DiNola, J.R. Haak, J. Chem. Phys. 81 (8) (1984) 3684.
[27] See e.g. N.W. Ashcroft, N.D. Mermin, Solid State Physics, Saunders, Philadelphia, 1976, Chapter 4.
[28] A.J.E. Foreman, W.J. Phythian, C.A. English, Rad. Eff. Def. Sol. 129 (1–2) (1994) 25.
[29] C.S. Becquart, C. Domain, A. Legris, J.-C.V. Duysen, J. Nucl. Mater. 280 (2000) 73.
[30] D. Terentyev, C. Lagerstedt, P. Olsson, K. Nordlund, J. Wallenius, L. Malerba, J. Nucl. Mater. 351 (2006) 65.
[31] M. Spaczér, A. Almazouzi, R. Schäublin, M. Victoria, Rad. Eff. Defect Sol. 141 (1997) 349.
[32] T.J. Colla, H.M. Urbassek, K. Nordlund, R.S. Averback, Phys. Rev. B 63 (2000) 104206.
[33] K. Nordlund, M. Ghaly, R.S. Averback, M. Caturla, T. Diaz de la Rubia, J. Tarus, Phys. Rev. B 57 (13) (1998) 7556.
[34] M. Ghaly, K. Nordlund, R.S. Averback, Philos. Mag. A 79 (4) (1999) 795.
[35] K. Nordlund, Comput. Mater. Sci. 3 (1995) 448.